

Article

Low Carbon Economic Dispatch of Integrated Energy System Considering Power-to-Gas Heat Recovery and Carbon Capture

Wenjin Chen ¹, Jun Zhang ¹, Feng Li ², Ruoyi Zhang ¹, Sennan Qi ³, Guoqing Li ⁴ and Chong Wang ^{4,*}¹ State Grid Zhejiang Electric Power Co., Ltd., Hangzhou 310063, China² China Electric Power Research Institute, Nanjing 210003, China³ Zhuji Power Supply Company of State Grid Zhejiang Electric Power Co., Ltd., Zhuji 311800, China⁴ College of Energy and Electrical Engineering, Hohai University, Nanjing 211100, China

* Correspondence: chongwang@hhu.edu.cn

Abstract: Carbon capture and storage (CCS) is an effective means to achieve the goals of carbon peaking and carbon neutrality. To improve the operating economics and low-carbon emission of an integrated energy system, the strong exothermic property of power-to-gas is utilized for heat recovery and injection into the heat network. This expands the adjustable range of electric output of combined heat and power (CHP) units which will improve wind power accommodation. The CO₂ produced by the coal-fired unit is captured using post-combustion carbon capture technology, and then stored and used to manufacture methane, in order to realize the electric–gas–heat integrated energy system coupled with power-to-gas. Based on the ladder-type carbon trading mechanism, a low-carbon economic dispatch model of integrated energy system is proposed, which considers the incorporation of power-to-gas heat recovery and carbon capture and storage. The objective function is to minimize the total operation cost of the system. The model is simulated in the revised IEEE 39-bus power network, Belgium 20-node gas network and 6-node heat network by CPLEX solver and simulation results verify the effectiveness of the proposed model.

Keywords: carbon capture and storage; integrated energy system; wind power accommodation; ladder-type carbon trading mechanism; power-to-gas heat recovery



Citation: Chen, W.; Zhang, J.; Li, F.; Zhang, R.; Qi, S.; Li, G.; Wang, C. Low Carbon Economic Dispatch of Integrated Energy System Considering Power-to-Gas Heat Recovery and Carbon Capture. *Energies* **2023**, *16*, 3472. <https://doi.org/10.3390/en16083472>

Academic Editor: Silvia Ravelli

Received: 20 February 2023

Revised: 5 April 2023

Accepted: 12 April 2023

Published: 15 April 2023



Copyright: © 2023 by the authors. Licensee MDPI, Basel, Switzerland. This article is an open access article distributed under the terms and conditions of the Creative Commons Attribution (CC BY) license (<https://creativecommons.org/licenses/by/4.0/>).

1. Introduction

With the acceleration of globalization, global crises such as the novel coronavirus epidemic and the Russia–Ukraine conflict have a huge impact on the energy system. To reduce the dependence on a single energy source, integrated energy systems with diversified energy sources should be constructed. Wang et al. [1] proposed that building a safe, efficient, clean and low-carbon new generation integrated energy system is one of the important means to achieve energy transformation and dual carbon goal. As mentioned in Li et al. [2] and Fan et al. [3], the two main technological paths are to increase the proportion of renewable energy and to implement various low carbon technologies. Wind power is abundant in north China, northeast China and northwest China. In these three regions, winter heating is generated by thermoelectric units, which are subject to the restriction of “determining electricity by heat” of combined heat and power (CHP). When the output of wind power is large, the output adjustment range of thermoelectric units is limited, resulting in a large amount of wind abandonment. Schneider et al. [4] proposed that power-to-gas (P2G) has the energy storage characteristics of time–space translation, which provides a solution for wind power absorption and peak shaving and effectively improves the flexibility of the integrated energy system. The research on P2G is mainly focused on the framework of an electric–gas integrated energy system. Ang et al. [5] optimized the sizing and siting of P2G facilities considering the uncertainties of carbon price and carbon tax. A co-optimization scheduling model of the two energy systems considering P2G was proposed by He et al. [6]. Wang et al. [7] built the carbon emission flow model which is used

to track the emission of P2G. Zhang et al. [8] considered gas-fired power and P2G to absorb renewable energy. P2G contributed to optimization as a part of the energy hub considered by He et al. [9]. To solve the problem of “determining electricity by heat”, researchers use heat storage devices and electric boilers for thermoelectric decoupling. Zeng et al. [10] proposed a gas storage life reliability model to characterize the performance. The investment cost of the heat storage device at the source side is high and the planned capacity is limited. It is difficult to absorb wind power on a large scale using only a heat storage device. Wang et al. [11] used gas turbines and electricity-to-natural gas facilities to address the uncertainty of renewable energy power generation. However, the low profit of P2G power stations have hindered the development of P2G. In fact, it is easy to understand that the methanation process has strong heat release characteristics from the chemical expression mentioned by Wang et al. [12]. Gotz et al. [13] proposed that the electricity-to-methane industrial chain can be incorporated into the heating application to improve efficiency. Considering the exothermic characteristics of P2G methanation reaction and injecting its reaction waste heat into the heat network, the coupling of electric–gas–heat network can be realized, and the economy and energy utilization rate of the system can be further improved. The design of the P2G integrated energy hub (P2G-EH) system is performed with a stochastic dynamic planning method by Alizad et al. [14]. Mansouri et al. [15] proved that P2G technology reduces CO₂ emissions by 9.89% through consuming CO₂ emitted from the CHP and boiler. Chaucy et al. [16] used a life cycle assessment methodology to prove that an integrated system will assess the most significant environmental impacts with P2G. A model containing P2G and energy storage was established to enhance the resilience of multi-carrier energy systems integrated with electric–gas–thermal networks by Hosseini et al. [17].

P2G methanation reaction uses electrolytic water to produce hydrogen and produces methane with CO₂ under the action of a catalyst, so the purchase of carbon is also an important part of P2G operation cost. At the same time, although the use of P2G and thermoelectric decoupling can effectively improve wind power consumption, the carbon emissions of thermal power units still need to be solved. Carbon capture and storage (CCS), as a low-carbon technology to cope with climate change, has great development potential and has been highly valued by countries around the world. The installation of carbon capture equipment in thermal power units can capture about 90% of CO₂ to store and utilize it. With the full use of existing units, it can realize low-carbon power generation, which to some extent reduces the grounding cost of existing fossil fuel units and the large investment in renewable energy power generation. Lee et al. [18] analyzes CCS cost reduction and its macroeconomic effects and shows that CCS can be economically feasible in the long term. A highly accurate surrogate model of CCS had been built for overall power consumption and separation responses by Ali et al. [19]. Reddy et al. [20] discussed the modeling and analysis of the carbon capture technology in emission-constrained environment. The low-carbon economic dispatch considering carbon capture power plant is solved in a multi-objective optimization framework by Akbari et al. [21]. Lou et al. [22] described a multi-period optimization model for carbon capture power plant.

With the increasing attention to carbon emission, carbon dioxide removal technologies have been developed rapidly. Sunghoon et al. [23] presented an advanced sub-ambient membrane process that improved CO₂/N₂ selectivity at low temperatures and reduced the cost of carbon capture. A solvent storage model had been proposed to improve the power plant’s ability to reduce power output while operating the CCS system, improving electricity sales revenue by Stefania et al. [24]. Du et al. [25] investigated the technical and economic feasibility of achieving zero and negative carbon dioxide emissions in pulverized coal and natural gas combined cycle power plants using conventional amine scrubbing using 30 wt% water ethanolamine. A mixture of ionic liquid and monoethanolamine (MEA) was proposed as a solvent choice with promising prospects for carbon dioxide removal technology by Akinola et al. [26]. Stefania et al. [27] proved that the capture level reduction mode is more economical than the traditional mode when applied to natural

gas power plants, reducing the economic disadvantage of carbon capture power plants. Yuan et al. [28] proved that after adding sulfolane or imidazole to the second-generation flue gas amine washing solvent, the circulation capacity of carbon dioxide increases, and the effect of capturing carbon dioxide increases. Liu et al. [29] proposed that the coupling of electrocatalytic technology and renewable energy is an important development direction in the future, which can improve the adsorption capacity of metal organic frameworks for carbon dioxide. Galina et al. [30] proved that pH change in mineral carbonation results in a carbon dioxide capture efficiency of 40–50%. Bielka et al. [31] designed a dehydration compression device that captures carbon dioxide after combustion, reducing the total energy consumption in CCS.

According to the above analysis, in response to the dual carbon goal, this paper introduces a ladder-type carbon trading mechanism from the perspective of low carbon, uses P2G heat recovery to realize the electricity–gas–heat network coupling and uses the CO₂ captured by CCS directly for methane production. At the same time, P2G and a heat storage tank can achieve thermoelectric decoupling and wind power consumption through collaborative operation, which realizes the low-carbon operation of the system and reduces CO₂ emissions and wind abandonment rate.

2. Electricity–Gas–Heat Integrated Energy System Model

The electric–gas–heat integrated energy system constructed in this paper includes carbon capture system, electric–gas–heat network and multiple coupling modules such as P2G, electric boiler (EB) and CHP. The excess heat can be recovered through the methanation process of P2G, and the CO₂ captured by the carbon capture device can be directly produced by P2G, which can reduce the carbon emission of the system and promote the consumption of wind power realizing the coupling of electricity, gas and heat networks. The model diagram of power–gas–heat integrated energy system is shown in Figure 1.

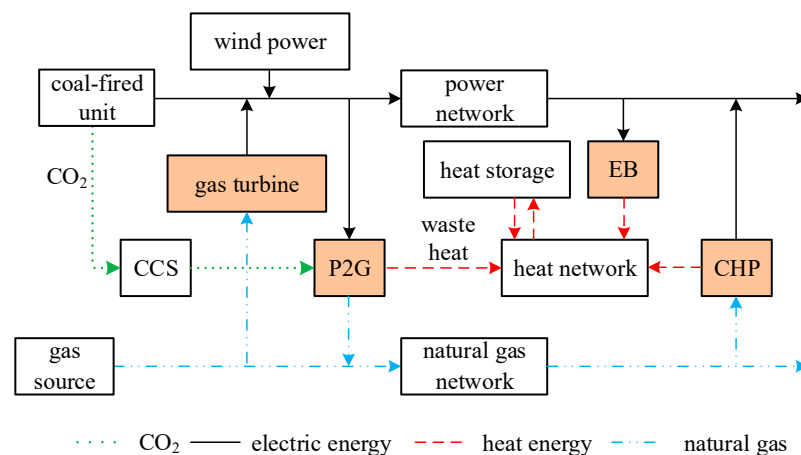


Figure 1. Model diagram of integrated energy system combined electricity, gas and heat.

2.1. P2G Model

P2G can be used as the electric load in the power network and the gas source in the natural gas network. In the process of methane production by P2G, a large amount of waste heat is generated, which can be used as the heat source in the heat network by its heat release characteristics. At the same time, P2G can directly use the CO₂ captured by the carbon capture device for production in the integrated energy system considering carbon capture. The reaction process of P2G to produce methane is as follows:



During the thermal reaction of methanation, 165.01 kJ of heat is released for every 1 mol of methane produced. The heat released by P2G can be collected through the heat exchanger and injected into the heat network.

The conversion relationship between CH₄ production rate of P2G and reaction heat release in unit time is as follows [13]:

$$V^{\text{CH}_4} = \frac{\rho_{\text{H}_2} \cdot P_{\text{P2G}} / v_{\text{H}_2}}{4M_{\text{H}_2}} \frac{M_{\text{CH}_4}}{\rho_{\text{CH}_4}} \cdot 10^3 \quad (2)$$

$$H_{\text{P2G},t} = \frac{\rho_{\text{H}_2} \cdot P_{\text{P2G}} / v_{\text{H}_2}}{4M_{\text{H}_2}} \frac{\Delta H \eta_{\text{P2G}}^{\text{heat}}}{3600} \quad (3)$$

where V^{CH_4} is the methane generation rate, v_{H_2} is the hydrogen generation rate, $v_{\text{H}_2} = 1 \text{ Nm}^3 / (3.47 \text{ kW} \cdot \text{h})$, M_{CH_4} and M_{H_2} are the molar mass of methane and hydrogen respectively, $M_{\text{CH}_4} = 16 \text{ g/mol}$, $M_{\text{H}_2} = 2 \text{ g/mol}$, ρ_{CH_4} and ρ_{H_2} are the density of methane and hydrogen, respectively, $\rho_{\text{CH}_4} = 717.4 \text{ g/Nm}^3$, $\rho_{\text{H}_2} = 89.9 \text{ g/Nm}^3$, P_{P2G} is the active power output of P2G power station, H_{P2G} is methanation heat reaction exothermic, ΔH is the value of heat released by the reaction when 1 mol of methane is generated, $\Delta H = 165.01 \text{ kJ}$, $\eta_{\text{P2G}}^{\text{heat}}$ is the proportion of methanation heat reaction injected into the heat network which is set to $\eta_{\text{P2G}}^{\text{heat}} = 0.8$ in Tanja et al. [32].

It can be calculated from the above equation that when the operating output of P2G is 1 MW, its reaction thermal output is:

$$H_{\text{P2G}} = \frac{89.9 \times 1 / 3.47}{4 \times 2} \frac{165.01 \times 0.8}{3600} = 0.1188 \text{ MW} \quad (4)$$

The thermal efficiency of methanation reaction can reach more than 10% and in the case it is worth implementing the heat recovery. Because the volume of CO₂ input and methane output before and after the reaction is the same. Therefore, the consumption of P2G is expressed as follows:

$$E_{\text{out},t} = \rho_{\text{CO}_2} V_t^{\text{CO}_2} = \rho_{\text{CO}_2} V_t^{\text{CH}_4} \quad (5)$$

where $E_{\text{out},t}$ is the amount of CO₂ consumed by P2G power station, ρ_{CO_2} is the density of CO₂, $V_t^{\text{CO}_2}$ is the volume of CO₂ input to P2G power station at time t , $V_t^{\text{CH}_4}$ is the volume of methane output from P2G power station at time t .

2.2. CHP Model

The cogeneration unit includes two types of units: back-pressure unit and steam extraction unit. The heat and power ratio of the steam extraction unit is adjustable, and the heat and power ratio of the back-pressure unit is fixed. The heat supply studied in this paper adopts the steam extraction unit, and Figure 2 shows its operation characteristics.

The operating range of the steam extraction cogeneration unit is ABCD. When the thermal power of the unit is at point h , the adjustable range of its electric power is between P_E and P_F . With the increase of thermal power, the adjustable range of its electric power gradually decreases. Due to the thermoelectric coupling characteristics of CHP, when there is wind abandonment in the system, it operates in the BC section state to minimize its own electrical output. However, when there are no other heat sources in the system, in order to meet the heat load supply requirements, the CHP thermal output cannot be reduced, making the forced electrical output of the CHP unable to further decrease, resulting in more severe wind abandonment.

According to the boundary vertex coordinates, the specific electrical power and thermal power of CHP under any working condition can be obtained:

$$\begin{cases} P_{\text{CHP},t} = \sum_{n=1}^4 \phi_{n,t} P_n \\ H_{\text{CHP},t} = \sum_{n=1}^4 \phi_{n,t} H_n \\ \sum_{n=1}^4 \phi_{n,t} = 1 \\ 0 \leq \phi_{n,t} \leq 1 \end{cases} \quad (6)$$

where $P_{\text{CHP},t}$ and $H_{\text{CHP},t}$ are the electrical and thermal power of the CHP unit at time t , $\phi_{n,t}$ is the operating point of the CHP unit at time t , P_n and H_n are the electrical and thermal power at the operating peak n .

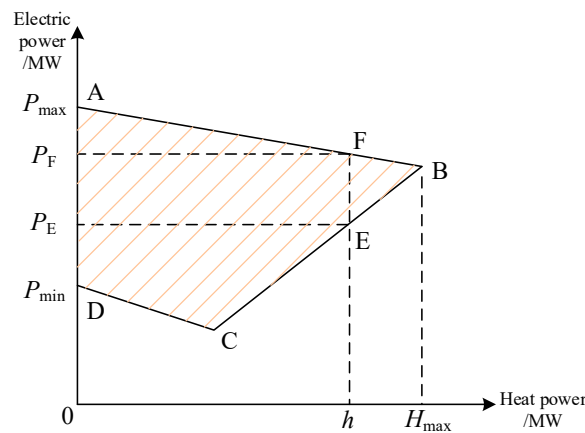


Figure 2. Operating characteristics of pumped heat and power system.

3. Low-Carbon Economic Dispatch of Integrated Energy System Considering P2G Heat Recovery and Carbon Capture

3.1. Carbon Capture System Model

Carbon capture technology is the core link of CCS. At present, thermal power plants mainly exist three ways: pre-combustion capture, post-combustion capture and oxygen-rich combustion decarbonization technology mentioned in Gładysz et al. [33] and Yin et al. [34]. The advantage of post-combustion capture technology is that it can directly transform the existing unit to install the capture equipment. It has been applied in some thermal power plants, and the captured carbon dioxide concentration is higher than 99%. In this paper, post-combustion capture and storage technology is used to deal with the carbon dioxide produced by coal-fired units. The total energy consumption of carbon capture system consists of basic energy consumption and operation energy consumption proposed by Yin et al. [35].

$$\begin{cases} P_{\text{CCS},t} = P_B + P_{\text{ON},t} \\ P_{\text{ON},t} = K_{\text{CCS}} E_{\text{CCS},t} \\ E_{\text{CCS},t} = \eta_{\text{CCS}} E_{C,t} \\ E_{C,t} = \delta_i P_{i,t} \end{cases} \quad (7)$$

where $P_{\text{CCS},t}$ is the total energy consumption of carbon capture device at time t , P_B is the basic energy consumption of carbon capture device, $P_{\text{ON},t}$ is the operating energy consumption of the carbon capture device at time t , which is proportional to the amount of CO_2 captured at the current time $E_{\text{CCS},t}$, K_{CCS} is the electrical power required to process unit CO_2 , $E_{\text{CCS},t}$ is the amount of CO_2 captured by the carbon capture device at time t , η_{CCS} is the capture efficiency of carbon capture device, $E_{C,t}$ is the actual carbon emission of the unit at time t , δ_i is the carbon emission intensity of unit i , $P_{i,t}$ is the output of unit i at time t .

Since CO₂ is always generated during the operation of the unit, the captured CO₂ usually needs to be stored or transported to the place of use by pipeline. This paper assumes that the pipeline has been laid by the investment operator. The system does not consider the pipeline investment cost and considers the transmission cost and storage cost of CO₂ transmission to P2G:

$$E_{store,t} = E_{store,t-1} + E_{CCS,t} - E_{out,t} - E_{ex,t} \tag{8}$$

$$f_{CCS} = \sum_{t=1}^T (C_{store}E_{store,t} + C_{tran}L_iE_{out,t}) \tag{9}$$

where $E_{store,t}$ is the carbon seal stock at time t , $E_{ex,t}$ is the amount of CO₂ discharged into the atmosphere due to the inability to use and store at time t , f_{CCS} is the cost of transmission and storage, T is the dispatch period, C_{store} is the cost required to store unit CO₂, C_{tran} is the cost required to transmit unit CO₂, L_i is the distance from the carbon capture point to the P2G.

3.2. Carbon Trading Model

3.2.1. Carbon Trading Quota

Under the carbon trading mechanism, the regulatory authority allocates carbon emission quotas for each carbon emission source in the system. According to the relevant national policies, the carbon emission quotas for each type of unit are different. The carbon emission quota $E_{B,t}$ of the system can be expressed as mentioned by Chalmers et al. [36]:

$$E_{B,t} = \sum_{i=1}^{N_{all}} \xi_i P_{i,t} \tag{10}$$

where ξ_i is the carbon emission quota reference value of unit i , N_{all} is the number of all units.

The carbon emission trading volume $E_{real,t}$ actually involved in carbon trading can be expressed as:

$$E_{real,t} = E_{C,t} - E_{CCS,t} - E_{B,t} + E_{ex,t} \tag{11}$$

3.2.2. Ladder-Type Carbon Trading Mechanism

Compared with the traditional carbon trading mechanism, the ladder-type carbon trading mechanism has strict control over carbon emissions. The ladder-type carbon trading mechanism is divided into several sections according to carbon emissions. Tabar et al. [37] showed that with the increase of carbon emissions, the corresponding unit carbon trading costs will also rise. From the actual carbon emissions of the system participating in carbon trading, we can get the ladder carbon trading cost as follows:

$$f_{tax,t} = \begin{cases} C_{tax}E_{real,t}, & E_{real,t} \leq l \\ C_{tax}[E_{real,t}(1 + \gamma_{tax}) - l\gamma_{tax}], & l \leq E_{real,t} \leq 2l \\ C_{tax}[E_{real,t}(1 + \gamma_{tax}) - 3l\gamma_{tax}], & 2l \leq E_{real,t} \leq 3l \\ C_{tax}[E_{real,t}(1 + \gamma_{tax}) - 6l\gamma_{tax}], & 3l \leq E_{real,t} \leq 4l \\ C_{tax}[E_{real,t}(1 + \gamma_{tax}) - 10l\gamma_{tax}], & E_{real,t} \geq 4l \end{cases} \tag{12}$$

where $f_{tax,t}$ is the stepwise carbon transaction cost of the system, C_{tax} is the system's carbon trading benchmark price, γ_{tax} is the growth rate of carbon tax, l is the interval length of total carbon emissions.

3.3. Objective Function

In this paper, the objective function is to minimize the total cost of the system:

$$\min F = f_1 + f_2 + f_3 + f_4 + f_{gas} + f_{tax} + f_{CCS} \tag{13}$$

where F is the total cost of the system, f_1 is the fuel cost of coal-fired units, f_2 is the start–stop cost of the unit, f_3 is wind abandonment cost, f_4 is the carbon purchase cost of P2G, f_{gas} is the system gas purchase cost.

3.3.1. Operating Cost of Coal-Fired Units

The operation cost of coal-fired units includes fuel cost and start–stop cost:

$$f_1 = \sum_{t=1}^T \sum_{i=1}^{N_F} (a_i P_{F,i,t}^2 + b_i P_{F,i,t} + c_i) \quad (14)$$

where N_F is the number of coal-fired units, a_i , b_i , and c_i are the quadratic fitting coefficients of the operation cost of coal-fired unit i , $P_{F,i,t}$ is the active output of coal-fired unit i at time t .

3.3.2. Start and Stop Costs

The CHP unit cannot shut down due to its heating task. Therefore, this paper only considers the startup and shutdown of coal-fired units and gas turbines, and the specific formula is as follows:

$$f_2 = \sum_{t=1}^T \sum_{i=1}^{N_G} u_{i,t}(1 - u_{i,t-1})C_{\text{open},i} \quad (15)$$

where N_G is the total number of coal-fired units and gas-fired units, $u_{i,t}$ and $u_{i,t-1}$ are, respectively, the operating states of the coal burning or gas generating unit i at time t . $u_{i,t} = 1$ means that it is in running state, $u_{i,t} = 0$ means that it is in shutdown state. $C_{\text{open},i}$ is the start-up cost of coal or gas unit i .

3.3.3. Gas Purchase Cost

Gas turbines and CHP units can be regarded as gas loads in the electric–gas–heat integrated energy system. Their fuel costs can be attributed to the gas source purchase cost. P2G can be regarded as a natural gas source, and its methane income is reflected in the gas consumption of the gas source.

$$f_{\text{gas}} = \sum_{t=1}^T \sum_{i=1}^{N_{\text{gas}}} \beta_i Q_{i,t}^{\text{gas}} \quad (16)$$

where N_{gas} is the number of air source points, β_i is the gas consumption cost coefficient of the i th gas source point. $Q_{i,t}^{\text{gas}}$ represents the air consumption at the i th air source point.

3.3.4. Cost of Wind Abandonment

The cost of wind abandonment is represented as follows.

$$f_3 = \sum_{t=1}^T C_{\text{curt}}(P_{\text{wind},t}^{\text{pre}} - P_{\text{wind},t}) \quad (17)$$

where C_{curt} is the wind abandonment penalty coefficient, $P_{\text{wind},t}^{\text{pre}}$ is the predicted output value of wind power at time t , $P_{\text{wind},t}$ is the actual output value of wind power at time t .

3.3.5. Carbon Purchase Cost

When P2G is supplied with no carbon source, additional carbon purchase costs need to be paid:

$$f_4 = \sum_{t=1}^T C_p E_{\text{out},t} \quad (18)$$

where C_p is the cost required to purchase unit CO_2 .

3.4. Constraints

3.4.1. Power Flow Constraints

The power network model mainly includes three parts [10]: constraints on node power balance, DC power flow constraints and minimum start–stop time constraints.

(1) Constraints on node power balance

$$\begin{aligned} & \sum_{i \in \Omega_F} P_{F,i,t} + \sum_{i \in \Omega_{GT}} P_{GT,i,t} + \sum_{i \in \Omega_{Wind}} P_{Wind,i,t} + \sum_{i \in \Omega_{CHP}} P_{CHP,i,t} + \sum_{l \in i} P_{l,t} \\ & = P_{load,i,t} + \sum_{i \in \Omega_{P2G}} P_{P2G,i,t} + \sum_{i \in \Omega_{EB}} P_{EB,i,t} + P_{CCS,t} \end{aligned} \tag{19}$$

where Ω_F is the set of all coal-fired generators, Ω_{GT} represents the collection of all gas turbines, Ω_{Wind} is the collection of all wind farms, Ω_{CHP} is the set of all CHP units, Ω_{EB} is the set of all electric boilers, Ω_{P2G} is a collection of all P2G devices, $l \in i$ is all the lines connected to node i , $P_{load,i,t}$ is the load power of node i at time t .

(2) Constraints on upper and lower limits of unit power

$$u_{i,t} P_i^{min} \leq P_i \leq u_{i,t} P_i^{max} \tag{20}$$

where P_i^{max} and P_i^{min} are, respectively, the maximum and minimum output values of unit i .

(3) Minimum start–stop time constraints

$$\begin{cases} \sum_{k=t}^{t+T_{off}-1} (1 - u_{i,k}) \geq T_{off}(u_{i,t-1} - u_{i,t}) \\ \sum_{k=t}^{t+T_{on}-1} u_{i,k} \geq T_{on}(u_{i,t} - u_{i,t-1}) \end{cases} \tag{21}$$

where T_{off} is the minimum shutdown time of the unit, T_{on} is the minimum shutdown time of the unit.

(4) Constraint on unit climbing rate

Unit climb rate constraints include coal-fired units, gas turbines and P2G power stations:

$$P_{i,t} - P_{i,t-1} \leq u_{i,t-1}(P_i^{up} - S_i^{up}) + S_i^{up} \tag{22}$$

$$P_{i,t} - P_{i,t-1} \leq u_{i,t}(P_i^{down} - S_i^{down}) + S_i^{down} \tag{23}$$

where P_i^{up} and P_i^{down} are, respectively, the lifting and falling output rates of unit i in continuous operation, S_i^{up} is the lifting output rate of unit i starting, S_i^{down} is the output reduction rate of unit i shutdown.

(5) DC power flow constraints

$$\begin{cases} \theta_n^{min} \leq \theta_n \leq \theta_n^{max} \\ P_{nl}^{min} \leq P_{nl} \leq P_{nl}^{max} \\ B_l(\theta_n - \theta_m) - P_{nl} = 0 \end{cases} \tag{24}$$

where θ_n^{max} and θ_n^{min} are the upper and lower limits of power angle of node n , respectively, P_{nl}^{max} and P_{nl}^{min} are the upper and lower limits of power on the road connected by node n , B_l is the equivalent susceptance of line l .

3.4.2. Natural Gas Network Constraints

The natural gas network model mainly includes three parts: gas source point, pipeline and pressure station (compressor). Natural gas is supplied through the gas source point, and then transmitted and distributed to the load through the pipeline. The pressure station can improve the node pressure and reduce the probability of natural gas clogging when the gas load peaks [10].

(1) Gas source point

The natural gas in the gas network is injected by the gas source point, and the gas flow output of each gas source point has upper and lower limits:

$$S_{\text{gas},s}^{\min} \leq S_{\text{gas},s,t} \leq S_{\text{gas},s}^{\max} \quad (25)$$

where $S_{\text{gas},s}^{\min}$ and $S_{\text{gas},s}^{\max}$ are, respectively, the minimum and maximum output flow of natural gas at the gas source point s .

(2) Natural gas pipeline

For the ideal adiabatic gas pipeline m and n , the beginning and end points are m and n , respectively, and the steady-state flow rate can be expressed as:

$$Q_{mn,t} = D_{mn,t} C_{mn} \sqrt{D_{mn,t} - (\psi_{m,t}^2 - \psi_{n,t}^2)} \quad (26)$$

$$D_{mn,t} = \begin{cases} 1 & , \psi_{m,t} \geq \psi_{n,t} \\ -1 & , \psi_{m,t} \leq \psi_{n,t} \end{cases} \quad (27)$$

where $Q_{mn,t}$ is the natural gas flow through pipeline mn at time t , C_{mn} is related technical parameter of pipeline, $\psi_{m,t}$, $\psi_{n,t}$ are the pressure values of the source points m and n at time t . $D_{mn,t}$ is the transmission direction of natural gas in the pipeline at time t , 1 is the positive direction, -1 is the negative direction.

Upper and lower limit constraints of pipeline flow:

$$Q_{mn}^{\min} \leq Q_{mn,t} \leq Q_{mn}^{\max} \quad (28)$$

where Q_{mn}^{\max} and Q_{mn}^{\min} are, respectively, the upper and lower limits of natural gas flow through pipeline mn .

Upper and lower limit constraints on pressure of each node:

$$\psi_m^{\min} \leq \psi_m \leq \psi_m^{\max} \quad (29)$$

where ψ_m^{\max} and ψ_m^{\min} are the upper and lower limits of pressure of node m , respectively.

(3) Compressor

The pressurizing station increases the pressure of the natural gas pipeline in which it is located. The most important part is the compressor. Ignoring the consumption characteristics of the compressor, the pressure relationship between the two ends of the compressor is as follows:

$$\psi_m = \rho_c \psi_n \quad (30)$$

where ψ_m and ψ_n are the pressure at the outlet and inlet of the compressor, respectively, ρ_c is the compression ratio of the compressor.

(4) Natural gas flow balance

According to the law of conservation of flow, the flow balance equation of each node in the natural gas network can be listed as follows:

$$\sum_{n \in m} Q_{mn,t} + Q_{\text{GT},m,t} + Q_{\text{CHP},m,t} + Q_{\text{load},m,t} = S_{m,t} + Q_{\text{P2G},m,t} \quad (31)$$

where $n \in m$ is all nodes adjacent to node m , $Q_{\text{GT},m,t}$ is the amount of natural gas consumed by the gas turbine connected to node m at time t , $Q_{\text{CHP},m,t}$ is the amount of natural gas consumed by the CHP unit connected to node m at time t , $S_{m,t}$ is the natural gas supply at time t of the gas source point connected to node m , $Q_{\text{P2G},m,t}$ is the gas load of node m at time t .

3.4.3. Heat System Constraints

The heat system mainly includes the constraint of heat source, heat network and heat storage device [12].

(1) Heat source model

The main heat sources are CHP units and electric boilers. The relevant constraints of CHP units are shown in Equation (6).

In the electric–gas–heat integrated energy system, the electric boiler is not only the electric load, but also the heat source. Its thermal output is expressed as follows:

$$H_{EB,t} = \eta_{EB}P_{EB,t} \tag{32}$$

where $H_{EB,t}$ is the thermal output of the electric boiler at time t , η_{EB} is the electrothermal conversion efficiency of electric boiler, which is 0.85.

(2) Heat network model

The heat subsystem is shown in Figure 3. The heating temperature $T_j^{ps,in}$ is the inlet water temperature of water supply pipeline A, heating temperature $T_j^{ps,out}$ refers to the outlet water temperature of water supply pipeline A, heat return temperature $T_j^{pr,in}$ is the inlet water temperature of return water pipeline A, the heat return temperature is the water temperature at the exit of the return water pipeline A, T_i^{ms} and T_i^{mr} are the mixing temperatures of water supply pipeline and return water pipeline at node i , respectively, w_{ij}^s and w_{ij}^r are the hot water flow in the water supply pipeline and the return water pipeline, respectively.

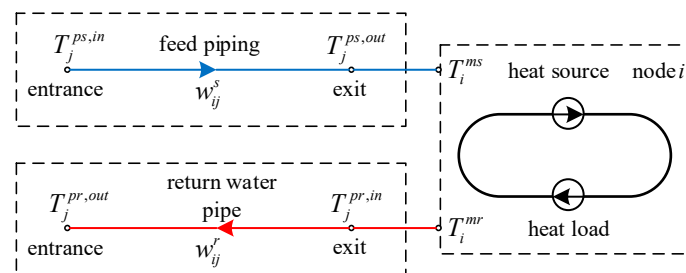


Figure 3. Thermodynamic subsystem model.

In the heat subsystem, the temperature relationship between hot water in multiple pipes before and after mixing with each other at a certain node can be expressed as:

$$\begin{cases} \sum_{j \in S_i^-} (T_j^{ps,out} w_{ij}^s) = T_i^{ms} \sum_{j \in S_i^-} w_{ij}^s \\ \sum_{j \in S_i^+} (T_j^{ps,out} w_{ij}^r) = T_i^{mr} \sum_{j \in S_i^+} w_{ij}^r \end{cases} \tag{33}$$

where $j \in S_i^-$ is a set of pipes with node i as the end, $j \in S_i^+$ is a collection of pipes starting with node i .

The temperature of hot water flowing out of node i is equal to the mixing temperature of the node:

$$\begin{cases} T_j^{ps,in} = T_i^{ms}, j \in S_i^+ \\ T_j^{pr,in} = T_i^{mr}, j \in S_i^- \end{cases} \tag{34}$$

Residential heating load is the most important heat load of heat subsystem. The expression of thermal load power is as follows:

$$H_{load,i} = C_p w_i (T_i^{ms} - T_i^{mr}) \tag{35}$$

where $H_{load,i}$ is the thermal load power of node i , C_p is the specific heat capacity of water, w_i injects water into node i of load node. T_i^{ms} is the heating temperature of node i after mixing, T_i^{mr} is the heat recovery temperature of node i after mixing.

In addition, the hot water flow in the thermal pipe should meet the conservation of flow, that is, the sum of the hot water flow out of each node is equal to the sum of the hot water flow in:

$$\sum_{j \in i} w_{ij} = 0 \quad (36)$$

(3) Heat storage device model

$$\begin{cases} H_{save,t} - H_{save,t-1} \leq H_{in}^{max} \\ H_{save,t-1} - H_{save,t} \leq H_{ex}^{max} \\ H_{save,t} \leq H_{save}^{max} \end{cases} \quad (37)$$

where $H_{save,t}$ and $H_{save,t-1}$ are the heat storage capacity of the heat storage device at time t and time $t-1$, respectively, H_{in}^{max} is the maximum heat storage power of the heat storage device, H_{ex}^{max} is the maximum heat discharging power of the heat storage device, H_{save}^{max} is the maximum heat storage capacity of heat storage device.

(4) Thermodynamic equilibrium

$$H_{CHP,t} + H_{EB,t} + H_{P2G,t} = H_{load,t} + H_{save,t} - H_{save,t-1} \quad (38)$$

3.4.4. Carbon Capture Related Constraints

In the carbon capture system, Zhou et al. [38] proposed that the total carbon storage in a cycle shall not exceed its upper limit:

$$E_{store,t} \leq E_{store}^{max} \quad (39)$$

where E_{store}^{max} is the maximum value of carbon storage capacity.

4. Case Study

4.1. Case Setting

The example in this paper is based on the interconnection network of 6-node heat network, 20-node gas network of Belgium and IEEE 39-bus power network. In this paper, the unit wind abandonment C_{cut} is set to 0.09 \$/(kW·h) in Li et al. [39]. In the ladder-type carbon trading mechanism, the system's carbon trading benchmark price C_{tax} is 30 \$/t, the growth rate of carbon tax γ_{tax} is 0.3 and the interval length of total carbon emissions l is 4×10^7 t in Moskalenko et al. [40]. The specific network structure diagram is shown in Figure 4. The 39-bus 10-unit power system has two wind power clusters, one CHP unit, two gas turbines and five coal-fired units. The CHP unit located at bus 30 of the power grid is connected to node three of the gas network and node one of the heat network, and the electric boiler located at bus 32 of the power grid is connected to node one of the heat network. P2G located at bus 31 of the power grid is connected to node seven of the gas network and node one of the heat network, gas turbines located at bus 33 and bus 37 of the power grid are connected to node six and node nineteen of the gas network, respectively, carbon capture devices are installed at bus 39 of the power grid. The CHP unit boundary vertex parameters are shown in Table 1. Electricity, heat, gas load and forecast output parameters of wind power are shown in Figures 5 and 6. In this paper, CPLEX solver was used to solve the problem, the time step was 1 h. The dynamic optimization results of one day and 24 h were analyzed.

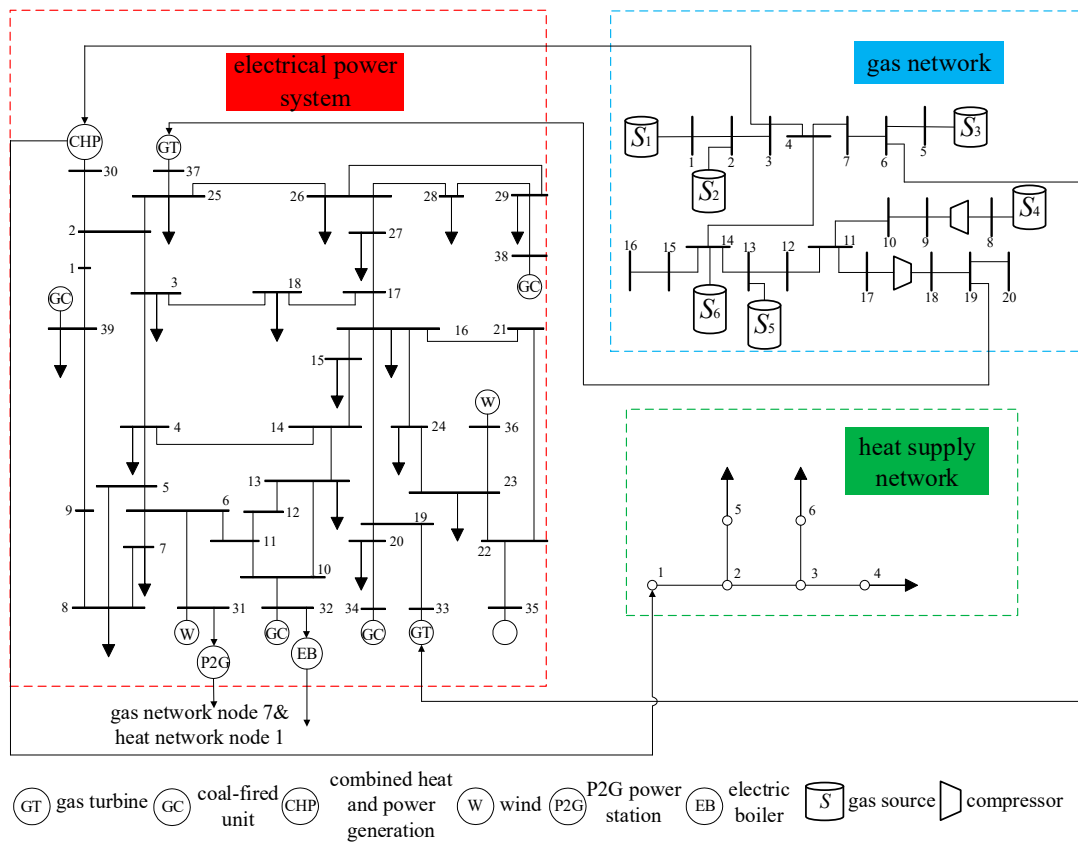


Figure 4. Electric-gas-heat integrated energy system structure diagram.

Table 1. Boundary vertex parameter of CHP.

Vertex Number	Electric Power/MW	Thermal Power/MW
1	81	104.8
2	215.0	180.0
3	247.0	0
4	98.8	0

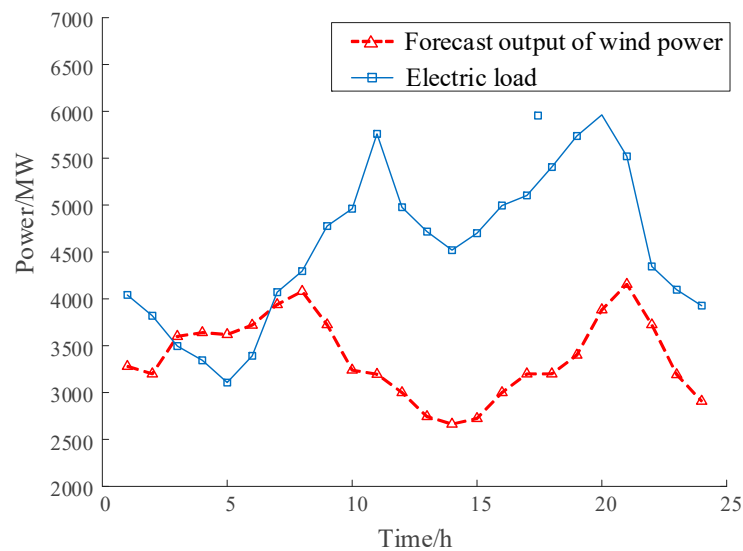


Figure 5. Output power forecasting of wind power and load.

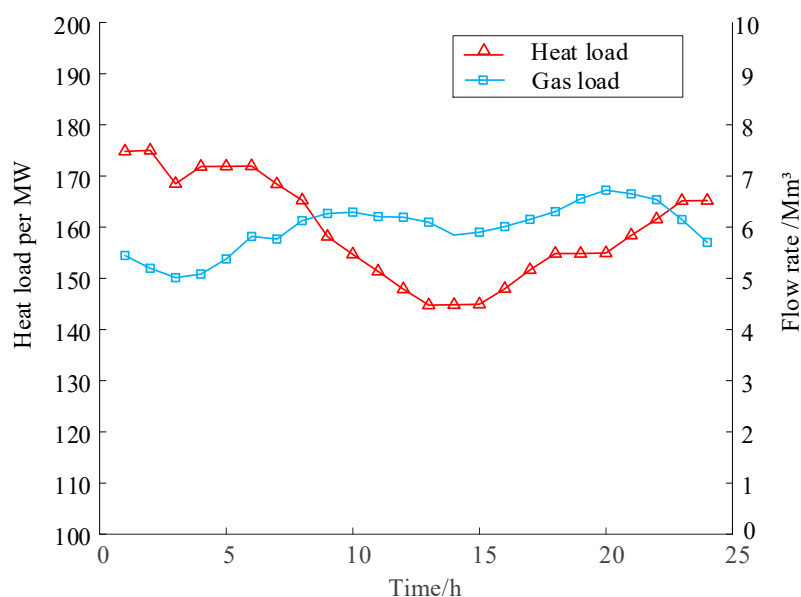


Figure 6. Output power of gas load.

In order to better compare the impact of each module on the low carbon and economy of the system, six scenarios are set up, as shown in Table 2.

Table 2. Module settings of each scenario.

Scenario	With CCS	With P2G	With Heat Recovery
1	×	×	×
2	×	✓	×
3	×	✓	✓
4	✓	×	×
5	✓	✓	×
6	✓	✓	✓

4.2. Simulation Results and Analysis

The results of low-carbon economy dispatch under six scenarios are shown in Table 3.

Table 3. Low-carbon economics dispatch results of different scenarios.

Scenario	1	2	3	4	5	6
Total cost/10 ⁴ \$	215.66	209.12	204.32	216.85	197.29	192.87
Coal-fired units operating cost/10 ⁴ \$	90.77	90.76	90.76	93.35	93.23	93.20
Gas purchase cost/10 ⁴ \$	69.03	67.82	65.91	64.41	63.10	60.74
Carbon purchase cost/10 ⁴ \$	/	4.04	3.86	/	0	0
Wind abandonment cost/10 ⁴ \$	16.50	7.12	5.63	16.50	5.41	3.77
Transmission and storage cost/10 ⁴ \$	/	/	/	10.13	7.62	8.12
Carbon trading cost/10 ⁴ \$	39.38	39.38	38.17	32.47	27.93	27.04
Methane production/m ³	/	71,462	68,317	/	83,819	80,103
Carbon emissions/t	8503.37	8501.16	8339.21	7615.59	6917.02	6731.78

As can be seen from Table 3, the electric output of the CHP unit is restricted because of “determining electricity by heat” and cannot be lowered, which results in a large amount of wind abandonment in Scenario 1. In Scenario 2, the total system cost is reduced by 3.03% after the introduction of P2G, mainly due to the absorption of a large amount of excess wind power during the wind abandonment period, which reduces 56.85% of the wind abandonment penalty cost. However, due to the need to meet the thermal balance

constraints, the electric output of CHP units cannot be further reduced at this time, and wind abandonment still exists. In Scenario 3, heat recovery of P2G is considered. P2G can not only generate income by using unused wind power to produce methane, but also inject residual heat from methanation into the heat network. P2G and its heat recovery relieved the heating pressure of CHP units and further reduced the forced electrical output, thus reducing the wind abandonment of the system. However, this also reduced the wind abandonment available for P2G to some extent and reduced the methane production of P2G by 4.4%. In Scenario 3, when wind curtailment exists, the system will preferentially use P2G power station for heating. If wind curtailment still exists, it will be supplied by electric boilers. When wind curtailment has been fully absorbed, the unmet heat load will finally be supplied by CHP units. In Scenario 3, when the electrical and thermal output of CHP units are both reduced, the gas purchase cost and actual carbon emissions of the units are also reduced. This result verifies that considering P2G and its heat recovery can improve the wind power consumption rate of the system and reduce the unit operating cost and carbon emissions. Figure 7 shows the wind discard characteristics in six scenarios.

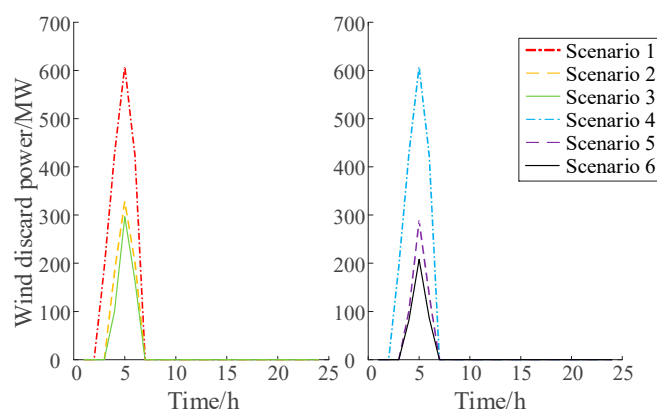


Figure 7. Wind power curtailment of different scenarios.

Compared with Scenarios 1, 2 and 3, Scenarios 4, 5 and 6 add carbon capture devices, and the output proportion of 39-bus coal-fired units increases. In Scenario 4, when wind curtailment exists in the system, coal-fired units at bus 39 will not operate because the power output of wind power and CHP has already met the power load requirements. Therefore, the carbon capture power output is zero and no more wind power can be absorbed. In the period without wind abandonment, carbon capture devices can capture a large amount of CO₂ to reduce carbon trading costs, but limited by storage capacity, the CO₂ that cannot be stored needs to be re-emitted into the atmosphere. Therefore, the reduced carbon transaction cost in Scenario 4 is very limited. The sequestered CO₂ is stored in large quantities for a long time, thus increasing the storage cost, and the total system cost is higher than that in Scenario 1.

After considering P2G power stations, Scenario 5 and Scenario 6 solve the problem of long-term storage of a large amount of CO₂. Compared with Scenario 4, the carbon trading costs are reduced by 13.98% and 16.72%, respectively, and the transmission and storage costs are reduced by 24.78% and 19.84%, respectively. In Scenarios 2 and 3, the operating cost of P2G is affected by the additional carbon purchase cost, which reduces the ability to consume wind power. In Scenarios 5 and 6, the methane production process of P2G is provided with carbon source by carbon capture device, without considering the additional carbon purchase cost, wind power and CO₂ can be consumed while generating income. Compared with Scenario 2 and Scenario 3, the abandonment cost is reduced by 24.02% and 43.52%, respectively. Figure 7 shows the thermal output of CHP units in Scenarios 5 and 6. As can be seen from Figure 8, when wind abandonment is severe (from 3 to 6), the thermal output of CHP unit in Scenario 6 is reduced, so that its forced electrical output continues to decrease, leaving more room for wind power consumption.

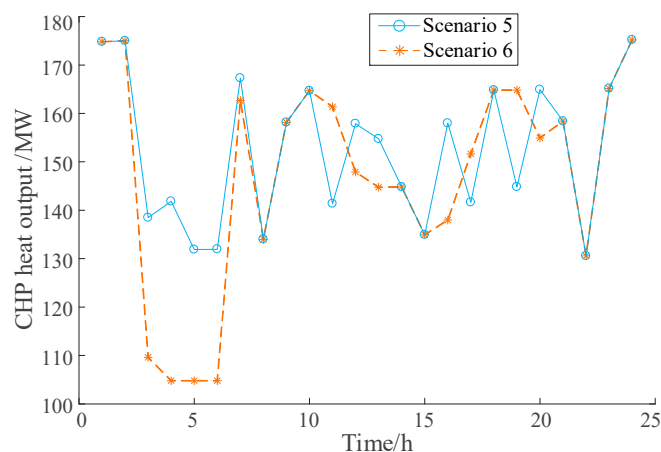


Figure 8. CHP heat output of Scenarios 5 and 6.

In conclusion, compared with the introduction of carbon capture, P2G and heat recovery alone, the optimized scheduling model of power–gas–heat integrated energy system proposed in this paper, which combines P2G heat recovery and carbon capture, has more significant effects on wind power consumption and CO₂ emission reduction.

4.3. Influence of Heat Storage Device on Operation Results

Based on Scenario 6, the influence of the heat storage device on the operating results of the system is analyzed. The operating results are shown in Table 4 and Figure 9, where the heat storage device is not considered in Figure 9a but is considered in Figure 9b.

Table 4. Impact of thermal energy storage on low-carbon economics dispatch.

Scenario	Total Cost /10 ⁴ \$	Wind Abandonment Cost /10 ⁴ \$
With thermal energy storage	192.87	3.77
Without thermal energy storage	195.61	3.83

As can be seen from Figure 9a, during the wind abandonment period, the heating output of the electric boiler has been full, and it cannot absorb more wind power. As can be seen from Table 3, after addition of the heat storage device, the CHP thermal output at 3 h in Figure 9b further decreases, thus reducing the penalty cost of wind abandonment. In the rest of the time, the use of heat storage devices can make the electrical and thermal output of the CHP unit more flexible and avoid the rigid coupling of thermoelectric to a certain extent reducing the total cost of the system by 1.4%.

4.4. Influence of P2G Capacity and Carbon Sequestration Capacity on Operation Results

This paper considers the combination of P2G heat recovery and carbon capture technology. However, in Scenario 4, due to the limitation of carbon sequestration capacity, a large amount of captured CO₂ is re-discharged, while in Scenarios 5 and 6, after removing the CO₂ consumed and sequestration of P2G methane production, some of the captured CO₂ can only be discharged. Moreover, wind abandonment cannot be fully absorbed due to the impact of P2G capacity ceiling in Scenario 6. Therefore, it is necessary to analyze the influence of different P2G capacity and carbon sequestration capacity configurations on system operation. The total system cost operation results under different capacity configurations are shown in Figure 10.

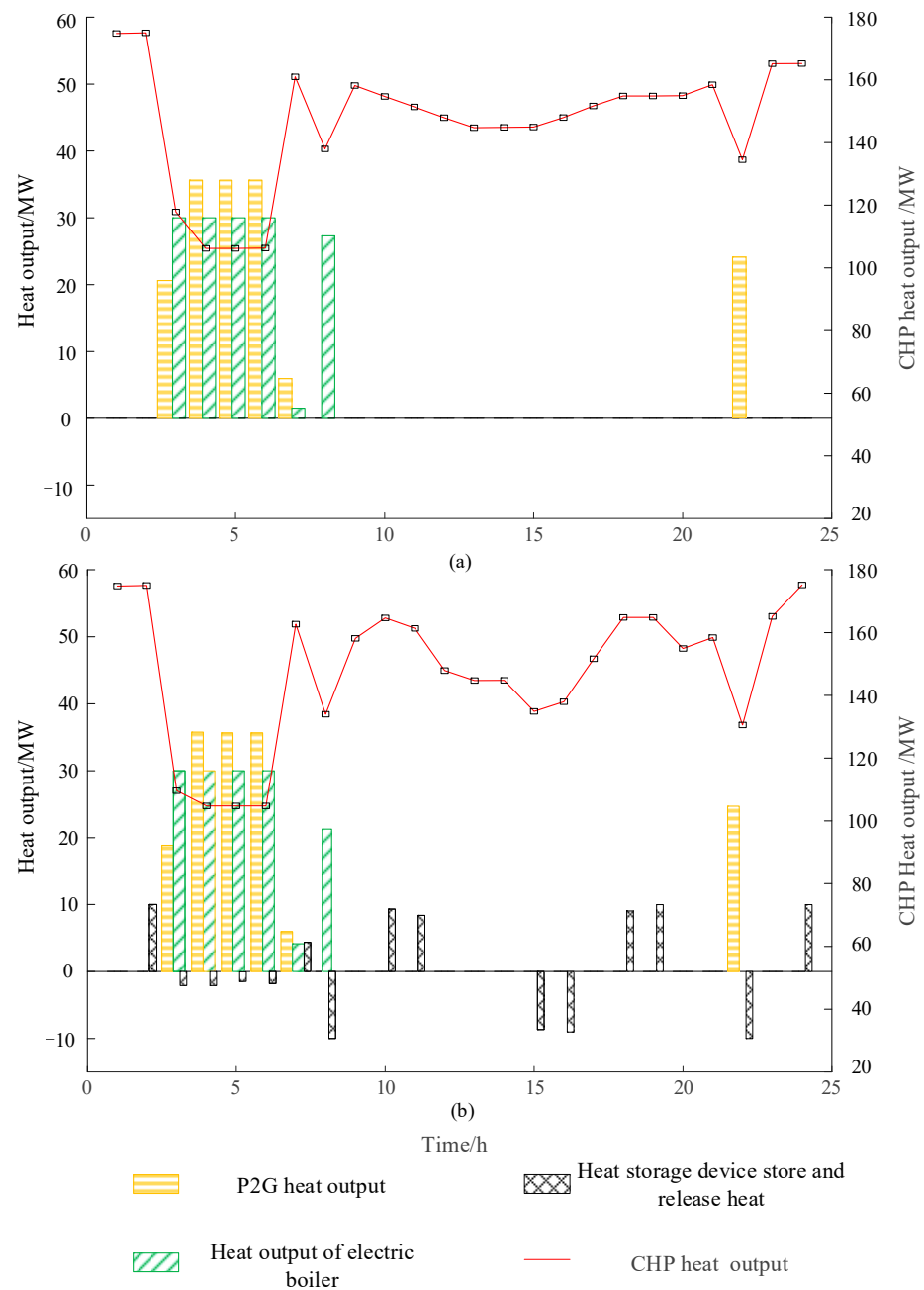


Figure 9. Effect of heat energy storage on heat output of the system. (a) Without heat storage device; (b) With heat storage device.

As can be seen from Figure 10, when the P2G capacity is lower than 500 MW, the system can absorb more wind power with the increase of P2G capacity, and the total system cost shows a downward trend. When the P2G capacity is greater than 500 MW, the total system cost will not be affected by the further increase of P2G capacity because the wind power has been fully absorbed.

When the carbon sequestration capacity is low, P2G incurs an extra carbon purchase cost, which affects its gas production efficiency. When the carbon sequestration capacity is high, CO₂ that is not sequestered decreases and in consequence the carbon transaction cost is reduced, resulting in a less system operational cost. When the carbon sequestration capacity is greater than 1900 t, P2G methane production and CO₂ obtained from sequestration and capture can be fully supplied, and the total cost of the system will not change.

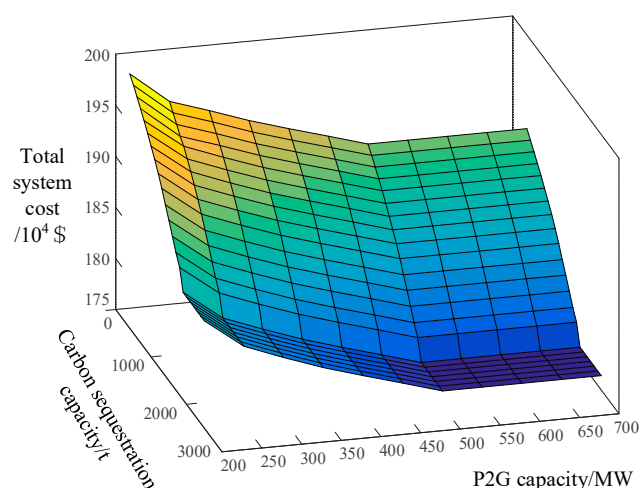


Figure 10. Total cost of different carbon storage capacity and P2G capacity.

5. Discussion

From the perspective of reducing carbon emission, this paper introduces the step carbon trading mechanism and constructs the model of electric thermal integrated energy system. In order to improve the economy, P2G heat recovery was used to achieve electrical and thermal coupling, and the carbon dioxide obtained from the carbon capture device was used for methane production. At the same time, P2G heat recovery and heat storage boiler improve the level of wind power consumption. The results show that the total operating cost of the whole system is reduced, and the carbon emission to the outside world is minimal. In addition, compared with the integrated energy system that does not consider P2G heat recovery, the wind power consumption of the whole system is improved.

The development of carbon capture technology is very rapid and considering more efficient carbon capture technology in the future will further reduce the carbon emissions of system operation [23,24]. In addition, this paper adopts a deterministic model, and the consideration of weather randomness and event randomness is the direction of future research. Among them, the commonly used models considering randomness include Markov model, chance-constraint programming and robust optimization model. In recent years, the emergence of random events, such as the novel coronavirus epidemic and the Russia–Ukraine conflict have had a great impact on the entire energy system. Therefore, considering the impact of random events on the comprehensive energy system and prevention of random events are future research topics. By considering extreme weather or extreme events, the elasticity of the integrated energy system will be improved.

6. Conclusions

Aiming at the dual carbon goal, this paper proposes a low-carbon economic optimization dispatch model of the electric–gas–heat integrated energy system, which considers P2G heat recovery and carbon capture. The influence of six scenarios combining the three factors of P2G, heat recovery and carbon capture on the system operation results is analyzed with examples. Sensitivity analysis of some parameters is carried out, and the following conclusions are obtained:

- (1) Neither CCS nor P2G heat recovery alone can achieve the low-carbon and economic optimization of the system. Combining P2G heat recovery with CCS can effectively improve the system's wind power consumption and reduce CO₂ emissions.
- (2) Considering the heat storage device, the operating flexibility of the CHP unit can be improved, and the total operating cost of the system can be reduced.
- (3) The larger the capacity of P2G and carbon sequestration capacity is not better. The wind power that P2G can absorb is limited. When its capacity is higher than 500 MW, the total cost of the system will not change. When carbon sequestration capacity

is increased by 1900 t, the excess CO₂ that is not used to produce methane can be sequestered by means of carbon sequestration. Although increasing carbon sequestration capacity can effectively reduce carbon trading costs, its high carbon sequestration costs cannot be ignored.

In summary, the conclusions obtained in this paper can provide a basis for a low-carbon economic scheduling scheme in electric–gas–heat network. The model proposed in this paper only analyzes the day-ahead economic scheduling of the coordinated operation of P2G heat recovery and carbon capture under specific conditions, without taking the investment and operation and maintenance costs of each module into consideration. The practical application needs further calculation and research. The subsequent work will be related to the investment cost and policy of carbon capture and P2G.

Author Contributions: Conceptualization, W.C. and J.Z.; methodology, J.Z.; software, F.L. and G.L.; validation, S.Q. and C.W.; formal analysis, W.C.; investigation, W.C.; resources, W.C.; data curation, J.Z.; writing—original draft preparation, J.Z. and C.W.; writing—review and editing, R.Z. and C.W.; visualization, W.C.; supervision, C.W.; project administration, W.C. All authors have read and agreed to the published version of the manuscript.

Funding: This research received no external funding.

Data Availability Statement: Data is unavailable.

Conflicts of Interest: The authors declare no conflict of interest.

References

1. Wang, T.; Wang, X.; Gong, Y.; Jiang, C.; Xiong, F.; Li, L.; Zhao, Y. Initial allocation of carbon emission permits in power systems. *J. Mod. Power Syst. Clean Energy* **2017**, *5*, 239–247. [[CrossRef](#)]
2. Li, Y.; Wang, C.; Li, G.; Wang, J.; Zhao, D.; Chen, C. Improving operational flexibility of integrated energy system with uncertain renewable generations considering thermal inertia of buildings. *Energy Convers. Manag.* **2020**, *207*, 112526. [[CrossRef](#)]
3. Fan, F.; Zhang, R.; Xu, Y.; Ren, S. Robustly Coordinated Operation of an Emission-free Microgrid with Hybrid Hydrogen-Battery Energy Storage. *CSEE J. Power Energy Syst.* **2022**, *8*, 11.
4. Schneider, L.; Kotter, E. The geographic potential of Power-to-Gas in a German model region—Trier-Amprion 5. *J. Energy Stor.* **2015**, *1*, 1–6. [[CrossRef](#)]
5. Ang, X.; Shen, X.; Guo, Q.; Sun, H. Two-stage planning for electricity-gas coupled integrated energy system with CCUS considering carbon tax and price uncertainty. *IEEE Trans. Power Syst.* **2021**, 1–13. [[CrossRef](#)]
6. He, C.; Liu, T.; Wu, L.; Shahidehpour, M. Robust coordination of interdependent electricity and natural gas systems in day-ahead scheduling for facilitating volatile renewable generations via power-to-gas technology. *Mod. Power Syst. Clean. Energy* **2017**, *5*, 375–388. [[CrossRef](#)]
7. Wang, Y.; Qiu, J.; Tao, Y.; Zhang, X.; Wang, G. Low-carbon oriented optimal energy dispatch in coupled natural gas and electricity systems. *Appl. Energy* **2020**, *280*, 115948. [[CrossRef](#)]
8. Zhang, Y.; Zheng, F.; Shu, S.; Le, J.; Zhu, S. Distributionally robust optimization scheduling of electricity and natural gas integrated energy system considering confidence bands for probability density functions. *Int. J. Electr. Power Energy Syst.* **2020**, *123*, 106321. [[CrossRef](#)]
9. He, C.; Wu, L.; Liu, T.; Shahidehpour, M. Robust co-optimization scheduling of electricity and natural gas systems via ADMM. *IEEE Trans. Sustain. Energy* **2016**, *8*, 658–670. [[CrossRef](#)]
10. Zeng, Z.; Ding, T.; Xu, Y.; Yang, Y.; Dong, Z. Reliability evaluation for integrated power-gas systems with power-to-gas and gas storages. *IEEE Trans. Power Syst.* **2020**, *35*, 571–583. [[CrossRef](#)]
11. Wang, C.; Gao, R.; Wei, W.; Shafie-Khah, M.; Bi, T.; Catalao, J.P.S. Risk-based distributionally robust optimal gas-power flow with wasserstein distance. *IEEE Trans. Power Syst.* **2018**, *34*, 2190–2204. [[CrossRef](#)]
12. Wang, X.; Huang, W.; Wei, W.; Tai, N.; Huang, Y. Day-ahead optimal economic dispatching of integrated port energy systems considering hydrogen. *IEEE Trans. Ind. Appl.* **2021**, *58*, 2619–2629. [[CrossRef](#)]
13. Götz, M.; Lefebvre, J.; Mörs, F.; Koch, A.; Graf, F.; Bajohr, S.; Reimert, R.; Kolb, T. Renewable power-to-gas: A technological and economic review. *Renew. Energy* **2016**, *85*, 1371–1390. [[CrossRef](#)]
14. Alizad, E.; Rastegar, H.; Hasanzad, F. Dynamic planning of Power-to-Gas integrated energy hub considering demand response programs and future market conditions. *Int. J. Electr. Power Energy Syst.* **2022**, *143*, 108503. [[CrossRef](#)]
15. Mansouri, S.; Nematbakhsh, E.; Ahmarinejad, A.; Jordehi, A.; Javadi, M.; Matin, S. A Multi-objective dynamic framework for design of energy hub by considering energy storage system, power-to-gas technology and integrated demand response program. *J. Energy Storage* **2022**, *50*, 104206. [[CrossRef](#)]

16. Chauvy, R.; Dubois, L.; Thomas, D.; De Guy, W. Environmental impacts of the production of synthetic natural gas from industrial carbon dioxide. *Sustain. Prod. Consum.* **2022**, *30*, 301–315. [[CrossRef](#)]
17. Hosseini, S.; Ahmarinejad, A.; Tabrizian, M.; Bidgoli, M. Resilience enhancement of integrated electricity-gas-heating networks through automatic switching in the presence of energy storage systems. *J. Energy Storage* **2022**, *47*, 103662. [[CrossRef](#)]
18. Lee, H.; Lee, J.; Koo, Y. Economic impacts of carbon capture and storage on the steel industry—A hybrid energy system model incorporating technological change. *Appl. Energy* **2022**, *317*, 119208. [[CrossRef](#)]
19. Ali, A.; Nayereh, H.; Jurandir, Y. Carbon capture and storage energy consumption and performance optimization using metamodelling and response surface methodology. *J. Energy Resour. Technol.* **2022**, *144*, 050901.
20. Reddy, S.; Panwar, L.; Panigrahi, B.; Kumar, R. Modeling of carbon capture technology attributes for unit commitment in emission-constrained environment. *IEEE Trans. Power Syst.* **2016**, *32*, 662–671. [[CrossRef](#)]
21. Akbari, A.; Mohammadi, B.; Zare, K.; Khalili, T.; Bidram, A. Economic-emission dispatch problem in power systems with carbon capture power plants. *IEEE Trans. Ind. Appl.* **2021**, *57*, 3341–3351. [[CrossRef](#)]
22. Lou, S.; Lu, S.; Wu, Y.; Kirschen, S. Optimizing spinning reserve requirement of power system with carbon capture plants. *IEEE Trans. Power Syst.* **2015**, *30*, 1056–1063. [[CrossRef](#)]
23. Sunghoon, L.; Jin-Kuk, K. Process-integrated design of a sub-ambient membrane process for CO₂ removal from natural gas power plants. *Appl. Energy* **2020**, *260*, 114255.
24. Stefania, M.; Laura, P. Operating the CO₂ absorption plant in a post-combustion unit in flexible mode for cost reduction. *Chem. Eng. Res. Des.* **2019**, *147*, 604–614.
25. Du, Y.; Gao, T.; Rochelle, G.; Bhowan, A. Zero- and negative-emissions fossil-fired power plants using CO₂ capture by conventional aqueous amines. *Int. J. Greenh. Gas Control.* **2021**, *111*, 103473. [[CrossRef](#)]
26. Akinola, T.; Oko, E.; Wang, M. Study of CO₂ removal in natural gas process using mixture of ionic liquid and MEA through process simulation. *Fuel* **2019**, *236*, 135–146. [[CrossRef](#)]
27. Stefania, M.; Laura, P. Fixed and Capture Level Reduction operating modes for carbon dioxide removal in a Natural Gas Combined Cycle power plant. *J. Clean. Prod.* **2020**, *254*, 120016.
28. Yuan, Y.; Gary, R. CO₂ absorption rate and capacity of semi-aqueous piperazine for CO₂ capture. *Int. J. Greenh. Gas Control.* **2019**, *85*, 182–186. [[CrossRef](#)]
29. Liu, E.; Lu, X.; Wang, D. A Systematic Review of Carbon Capture, Utilization and Storage: Status, Progress and Challenges. *Energies* **2023**, *16*, 2865. [[CrossRef](#)]
30. Galina, N.; Arce, G.; Maroto-Valer, M.; Ávila, I. Experimental Study on Mineral Dissolution and Carbonation Efficiency Applied to pH-Swing Mineral Carbonation for Improved CO₂ Sequestration. *Energies* **2023**, *16*, 2449. [[CrossRef](#)]
31. Bielka, P.; Kuczyński, S.; Nagy, S. CO₂ Compression and Dehydration for Transport and Geological Storage. *Energies* **2023**, *16*, 1804. [[CrossRef](#)]
32. Tanja, S.; Jochen, G.; Markus, R.; Tobias, R. Methanation of CO₂-storage of renewable energy in a gas distribution system. *Energy Sustain. Soc.* **2014**, *4*, 2.
33. Madejski, P.; Chmiel, K.; Subramanian, N.; Kuś, T. Methods and Techniques for CO₂ Capture: Review of Potential Solutions and Applications in Modern Energy Technologies. *Energies* **2022**, *15*, 887. [[CrossRef](#)]
34. Gładysz, P.; Strojny, M.; Bartela, L.; Hacaga, M.; Froehlich, T. Merging Climate Action with Energy Security through CCS—A Multi-Disciplinary Framework for Assessment. *Energies* **2023**, *16*, 35. [[CrossRef](#)]
35. Yin, C.; Huang, Z. The development of carbon capture and storage in China: Progress, challenge and collaboration. In Proceedings of the 2018 Portland International Conference on Management of Engineering and Technology (PICMET), Honolulu, HI, USA, 19–23 August 2018.
36. Chalmers, H.; Gibbins, J. Initial evaluation of the impact of post-combustion capture of carbon dioxide on supercritical pulverised coal power plant part load performance. *Fuel* **2007**, *86*, 2109–2123. [[CrossRef](#)]
37. Tabar, V.; Hagh, M.; Jirdehi, A. Achieving a nearly zero energy structure by a novel framework including energy recovery and conversion, carbon capture and demand response. *Energy Build.* **2021**, *230*, 110563. [[CrossRef](#)]
38. Zhou, X.; Zhao, Q.; Zhang, Y.; Sun, L. Integrated energy production unit: An innovative concept and design for energy transition toward low-carbon development. *CSEE J. Power Energy Syst.* **2021**, *7*, 1133–1139.
39. Li, G.; Wang, C.; Lei, S.; Wang, X. Bi-level optimal allocation of power system considering carbon capture technology. *Electr. Power Autom. Equip.* **2023**, *43*, 25–31.
40. Moskalenko, N.; Lombardi, P.; Komarnicki, P. Multi-criteria optimization for determining installation locations for the power-to-gas technologies. In Proceedings of the 2014 IEEE PES General Meeting | Conference & Exposition, National Harbor, MD, USA, 27–31 July 2014; pp. 1–5.

Disclaimer/Publisher’s Note: The statements, opinions and data contained in all publications are solely those of the individual author(s) and contributor(s) and not of MDPI and/or the editor(s). MDPI and/or the editor(s) disclaim responsibility for any injury to people or property resulting from any ideas, methods, instructions or products referred to in the content.